The role of salinity in fluvio-deltaic morphodynamics: A long-term modelling study

Zeng Zhou[1,2], Luying Chen[3], Jianfeng Tao*[1,3], Zheng Gong[1,2], Leicheng Guo[4], Mick van der Wegen[5], Ian Townend[3,6], and Changkuan Zhang[3]

[1]State Key Laboratory of Hydrology-Water Resources and Hydraulic Engineering, Hohai University, Nanjing, China

[2]Jiangsu Key Laboratory of Coast Ocean Resources Development and Environment Security, Hohai University, Nanjing, China

[3]College of Harbour, Coastal and Offshore Engineering, Hohai University, Nanjing,China

[4]State Key Laboratory of Estuarine and Coastal Research, East China Normal University, Shanghai, China

[5]IHE Delft and Deltares, Delft, Netherlands

[6]Ocean and Earth Sciences, University of Southampton, UK

Abstract

Salinity difference between the terrestrial river discharge and the oceanic tidal water plays a role in modifying the local flow field and, as a consequence, estuarine morphodynamics. Although widely recognized, recent numerical studies exploring the long-term morphological evolution of river-influenced estuaries with two-dimensional, depth-averaged models have mostly neglected salinity. Using a three-dimensional morphodynamic model, we aim to gain more insight into the effect of salinity on the morphodynamics of fluvio-deltaic systems. Model results indicate that the resultant estuarine morphology established after 600 years differs

*Corresponding author. Email: aoetao@hhu.edu.cn

remarkably when a salinity gradient is included. A fan-shaped river-mouth delta exhibits less seaward expansion and is cut through by narrower channels when salinity is included. The inclusion of salinity tends to generate estuarine circulation which favours landward sediment transport and hence limits the growth of the delta while enhances the development of intertidal areas. The formation of deltaic channel-shoal patterns resulting from morphodynamic evolution tend to strengthen the salinity stratification which is characterised by an increased gradient Richardson number. The direction of the depth-averaged residual sediment transport over a tide may be opposite to the direction of residual velocity, indicating the significant influence of baroclinic effects on the net sediment transport direction (and hence morphological change). The effect of salinity on morphological evolution becomes less profound when the strength of tidal or fluvial forcing is dominant over the other. The effects of sediment type and flocculation, which are particularly important when salinity gradients are present, are also discussed. Overall, this study highlights that neglecting salinity to simulate long-term estuarine morphodynamics requires more careful justification, particularly when the environment is characterized by fine sediment types (favouring suspended transport), and relatively large river discharge and estuarine depth (favouring baroclinic effects).

Keywords: estuarine morphodynamics; salinity gradients; baroclinic effect; long-term morphodynamic modelling; fluvio-deltaic systems

1 Introduction

Estuarine morphodynamics has been a long-standing research focus because of its high scientific relevance and important socio-economic implications (Hibma et al, 2004). Depending on the hydrological and geological settings, different estuarine systems worldwide may exhibit a variety of morphologies and geometric characteristics. Apart from the inherent geologic reasons, these distinctive landforms are mostly the result of

the nonlinear interactions between various natural and anthropogenic processes operating over different temporal and spatial scales (Dalrymple and Choi, 2007; Townend, 2012). To understand these interactions and predict future morphodynamic evolution, the development of process-based models (also termed as “simulation models”, see, e.g. Murray, 2003) has expanded rapidly with the development of computer capabilities. Besides the relatively low cost, the advantages of using simulation models for the research on estuarine morphodynamics is the ability to examine the interacting processes selectively and at a range of space and time scales (Coco et al, 2013; Zhou et al, 2017).

Coupling a variety of governing equations, simulation models are capable of capturing these nonlinear dynamics, and hence are able to provide fundamental insight into the underlying mechanisms. The development of morphological acceleration approaches has further enhanced studies of long-term estuarine morphodynmaic behaviour (Roelvink, 2006). The numerical studies by Wang et al (1995) and Hibma et al (2003a,b) are among the first to simulate the formation and long-term development of two-dimensional channel-shoal patterns in estuaries and tidal basins. van der Wegen and Roelvink (2008) further extended this type of studies by investigating channel-shoal dynamics over millennia. Using the Western Scheldt estuary as an example, they found that the geometric characteristics of the simulated estuary (e.g. hypsometry, bar length) are qualitatively in agreement with the observed natural system (van der Wegen and Roelvink, 2012). The same model was later adopted by Zhou et al (2014b,c) to investigate the morphodynamics of back-barrier systems, in comparison to controlled laboratory experiments.

The above-mentioned studies mostly focused on tide-dominated systems with negligible river influence. As a step forward, Zhou et al (2014a) further included the riverine processes and demonstrated that the relative strength of tidal and fluvial discharges (in terms of both water and sediment) governs the evolution and the eventual fate of short

back-barrier systems. Guo et al (2015a,b) explored the hydrodynamic and morphodynamic behaviors of strongly river-influenced systems numerically, with the Yangtze estuary delta as a study case (Figure 1a). The model simulated the gradual formation of a non-cohesive sandy fluvio-deltaic system with meandering channels in the estuarine part and distributary channels in the deltaic part. In contrast, Braat et al (2017) investigated the role of cohesive mud supply to the large-scale estuarine morphology using an idealised model configuration, and suggested that mud favours shallower sides of estuaries and leads to narrower channels.

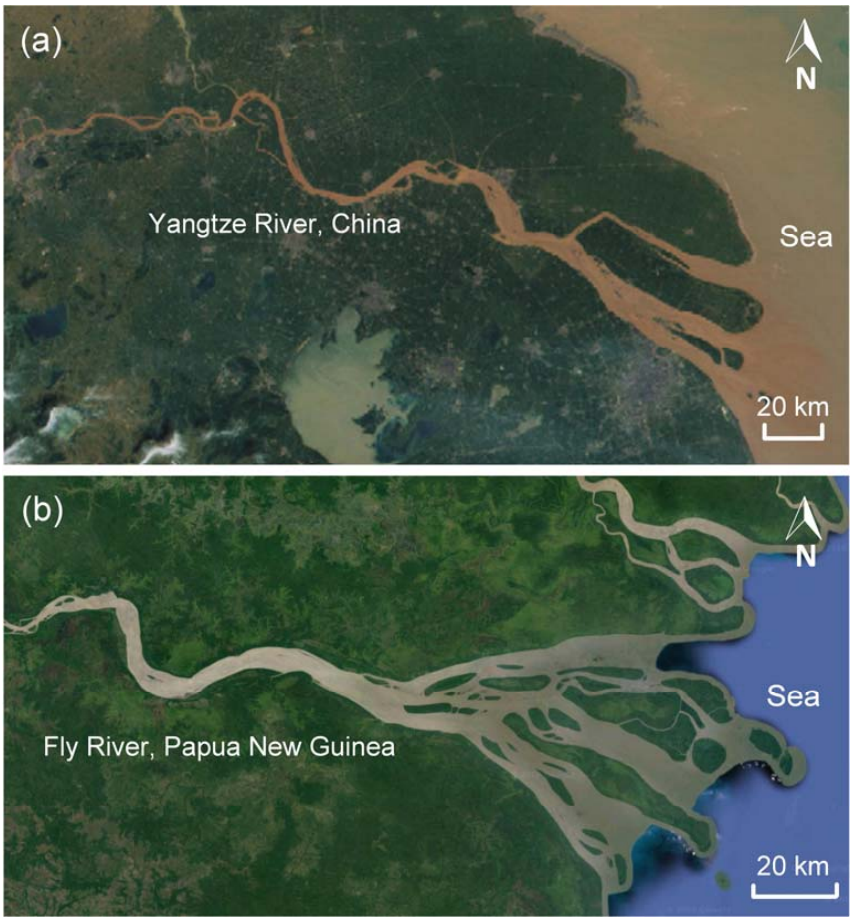

Figure 1: Typical examples of fluvio-deltaic systems under the combined influence of tidal and fluvial forcing: (a) the Yangtze River estuary, China, and (b) the Fly River estuary, Papua New Guinea. The figure is modified from ©GoogleMaps.

Although a river discharge has been added in these models, the related salinity gradients between the sea and the river have been only sporadically considered. Using

the Suisun Bay, California as a study case, Ganju et al (2009) demonstrated a morphodynamic hindcasting of decadal estuarine bathymetric change with salinity included. Since the focus of Ganju et al (2009) was not directly on salinity gradients, simulations excluding it were not reported and hence its morphodynamic influence could not be deduced. A later morphodynamic study of decadal timescale by van der Wegen et al (2011), focusing on a fairly close location (San Pablo Bay, California), suggested that the inclusion of salinity in the model led to better results compared to measured data. The evident stratification measured in this region indicated the importance of salinity gradients (Monismith et al, 2002), and hence its impacts on morphological evolution were accounted for in these studies (Ganju et al, 2009; van der Wegen et al, 2011; van der Wegen and Jaffe, 2014). In fact, many studies from the research communities of hydrodynamics and sediment dynamics, have also demonstrated that salinity gradients are strongly linked to commonly-observed estuarine phenomena, such as salt intrusion, lateral sediment entrapment, flocculation, estuarine turbidity maximum, and landward tide-residual sediment transport (Burchard and Baumert, 1998; Huijts et al, 2006; Gong and Shen, 2011). These phenomena, to some extent, are also linked with estuarine morphological changes over a long term. The main reason for neglecting salinity in long-term morphodynamic simulations has been mainly related to the considerable computational time required to run models in the three-dimensional (3D) mode (Zhou et al, 2014a; Guo et al, 2015b).

To the authors' knowledge, the long-term implication of neglecting salinity in simulation models has rarely been examined, leading to the question whether salinity can be neglected or not, or, when salinity may be neglected. Recently, Olabarrieta et al (2018) conducted a pioneering study on this using a three-dimensional (3D) morphodynamic model (ROMS) and they found that salinity gradient-driven baroclinic flows can have leading effects on morphodynamics of estuaries. In particular, their model results suggested that baroclinic effects can promote the import of sediment into the estuary,

accelerate the evolution of the upper/middle estuary, and tend to generate asymmetric morphologies. Inspired by the work of Olabarrieta et al (2018), this study aims to explore the role of salinity driven density differences on the long-term evolution of a fluvio-deltaic system with a similar morphology as Figure 1, using a different morphodynamic model (Delft3D). Differently from Olabarrieta et al (2018) who mainly focused on the estuary part (i.e. from the river boundary to the estuary mouth), the emphasis of this study is on the transition area near the estuary mouth with a specific focus on the delta. The specific research objectives include (1) to investigate the spatial and temporal variation of salinity gradients, (2) to compare the resultant long-term morphologies with and without salinity, and (3) to unravel how the role of salinity depends on the parameter space (e.g. river discharge, tidal range, settling velocity). By addressing these objectives, this contribution helps to shed light on the physical mechanisms underlying the role of salinity gradients on sediment transport and morphodynamic feedback of fluvio-deltaic systems over a long timescale from decades to millennia.

2 Methodology

The open-source morphodynamic model Delft3D is adopted for this study. Below, we will first briefly introduce the model and then detail the model parametrizations.

2.1 Numerical model description

The model consists of several coupled modules. For flow, it solves the two-dimensional (2D, depth-averaged) or 3D non-linear Navier-Stokes equations for incompressible fluid under the shallow water and the Boussinesq eddy viscosity assumptions, resulting in a detailed description of velocities and water levels over the model domain. The Coriolis effect is neglected to gain more direct understanding of the baroclinic effect on morphodynamics. In the horizontal direction, orthogonal curvilinear coordinates are used.

For 3D models, the vertical velocities are obtained from the continuity equation, and neglecting the vertical accelerations in the momentum equations. When the 3D mode is switched on, the so-called σ (sigma) coordinates are used in the vertical direction (Stelling and Van Kester, 1994).

The obtained flow velocities are then utilized to compute sediment transport. A variety of sediment transport formulas have been included in the model, and both sand and mud fractions can be considered. The estuarine environment is normally characterized by fine and cohesive sediment, so mud is considered in this study unlike several existing studies (e.g. Zhou et al, 2014a; Guo et al, 2015b). Fine sediment is treated as suspended load which can be highly affected by baroclinic effects induced by salinity gradients (Dalrymple and Choi, 2007). The cohesive sediment transport is modeled using an advection-diffusion equation in the model, with source and sink terms to describe erosion and deposition, respectively (Partheniades, 1965). It is worthwhile to mention that the bed slope effect as normally taken into account for bed load transport is not considered for mud transport. Cohesive mud can consolidate, leading to an increase in critical shear stresses for erosion and a reduction in bed levels (Zhou et al, 2016). Consolidation is not considered in this study for simplicity.

Cohesive sediment may also flocculate depending on the degree of salinity, resulting in aggregated particles which can settle more rapidly. To account for this effect, the model calculates the sediment settling velocity which is formulated as a function of the salinity of the water (Deltares, 2014). In this study, flocculation is considered in several simulations to illustrate its effect. It is worth noting that other parameters such as sediment concentration and composition may also play a role on flocculation (e.g. Manning et al, 2011). The effect of flocculation is considered by modifying the settling velocity of cohesive sediment, which is formulated as a function of the salinity of the water:

$$w_{\mathrm{s}} = \begin{cases} \frac{w_{\mathrm{sm}}}{2}\left[1-\cos(\frac{\pi S_{\mathrm{w}}}{S_{\max}})\right] + \frac{w_{\mathrm{s0}}}{2}\left[1+\cos(\frac{\pi S_{\mathrm{w}}}{S_{\max}})\right}, & \text{if } S_{\mathrm{w}} \leq S_{\max} \\ w_{\mathrm{sm}}, & \text{if } S_{\mathrm{w}} > S_{\max} \end{cases} \quad (1)$$

where w_{s0} is the settling velocity in fresh water (m/s), w_{sm} is the maximum settling velocity in saline water (m/s), S_{w} is the salinity of the water (ppt), $S_{\max}$ is the maximal salinity at which w_{sm} is specified ($S_{\max}$ = 31 ppt). Turbulence-induced flocculation and the break-up of flocs are not considered.

The calculated vertical sediment fluxes and the spatial gradient in horizontal sediment fluxes lead to a morphological change which is updated every hydrodynamic time step. The obtained new bed elevation is considered to update the flow field at the next hydrodynamic time step. A morphological acceleration factor, which linearly scales up the bed level change calculated at every hydrodynamic time step, is used to bridge the gap between hydrodynamic and morphological time scales and hence reduce the computational time (Roelvink, 2006).

For more details of the morphodynamic model, the reader is referred to Lesser et al (2004) and van der Wegen and Roelvink (2008).

2.2 Model configurations

A schematic model bathymetry of an exponentially convergent estuary is designed following Guo et al (2015b). To prevent the flood tide from reaching the river boundary, a relatively long estuary of approximately 800 km is considered (Figure 2, *x*- and *y*-directions respectively represent along- and across-estuary directions). Initially, a thick mud layer of 50 m is prescribed over the entire model domain to ensure sufficient sediment to be eroded until the non-erodible rock layer, acting implicitly as riverine sediment source to nourish the delta. At the seaward boundary, the water depth is set to 50 m and linearly decreases to 15 m at the estuary mouth, and further varies linearly

to 10 m at the river boundary where the mud concentration is set to zero (i.e. no mud is carried into the system by the river discharge) so as to make the model as transparent as possible. Outside the estuary mouth, the offshore domain is characterized by a wide basin mimicking a shallow continental shelf which can accommodate the potential development of the ebb delta. The offshore C-shaped sea boundary is forced by the semi-diurnal harmonic tidal level (with a period of 12 hours and a phase of 0 degree). The two cross-shore sea boundaries are prescribed by Neumann boundary conditions with zero alongshore water level gradients. The salinity at these sea boundaries is set to 30 ppt (parts per thousand). Because of the curvilinear grid adopted, the model has a fine resolution inside the estuary (cell size of 50-200 m) and a relatively coarse resolution at the seaward boundary (cell size of up to 2000 m). The total number of grid cells is 182834 (being the product of x- and y-direction resolutions, 1618×113).

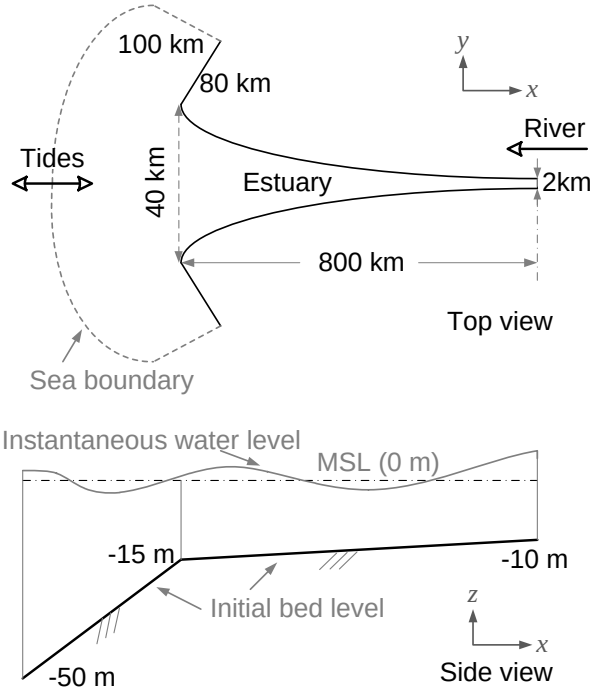

Figure 2: Schematic view of the model domain with dimensions similar to Guo et al (2015b). Note that the scales are distorted in the plot.

In the vertical direction, 10 σ layers are used and their relative thicknesses from the bottom to the free surface are 2, 3, 4, 6, 8, 10, 12, 15, 20, 20 % of the water depth

following the general guideline of the Delft3D model user manual (Deltares, 2014). The fine resolution at the bottom ensures a good representation of flow structure and sediment concentration near the bed where the vertical gradients of velocity and sediment concentration are strongest.

A series of simulations is designed by varying, e.g. the tidal/fluvial conditions, the calculation mode (2D or 3D) and sediment properties. Both 2D and 3D simulations are set up for comparison, shedding light on the role of salinity. A neutral 3D morphodynamic simulation is designed without considering salinity, in order to compare the differences among three settings: (a) 2D mode, (b) 3D mode without salinity, and (c) 3D mode with salinity. An overview of simulations is provided in Table 1. The model is run in parallel with multiple processors in a high-performance cluster. However, the long-term 3D runs with morphological updating still require a significant amount of time to complete, so a fixed bed is used for a number of short-term simulations focusing on hydrodynamics, salinity distribution and suspended sediment concentration. These simulations can help to gain in-depth insights into the (hydro- and sediment- dynamic) processes responsible for the resultant morphologies.

Table 1: Overview of designed simulations. In the type column, the capital letter 'HS' stands for 'hydrodynamics and sediment dynamics' (but no bed level change), and 'M' for 'morphodynamic update' (including hydrodynamics and sediment dynamics), e.g. 'HS2D' = 2D model of hydrodynamics and sediment dynamics, 'M3D-Floc' = 3D model of morphodynamic update accounting for flocculation. All these 3D simulations consider salinity except the one indicated by 'M3D-NS' which is a neutral morphodynamic simulation with no salinity. The parameters TR, Q and w_s indicate tidal range, fluvial discharge and sediment setting velocity, respectively. Flocculation is considered if w_s is varying between 0.25 and 0.5 mm/s.

Type	TR (m)	Q (10^3 m^3/s)	w_s (mm/s)
HS2D, HS3D	1.6, 2.0, 2.4 or 3.2	15	0.25
M2D	1.6, 2.0, or 2.4	10, 15, or 25	0.25
M3D-NS	2.4	15	0.25
M3D	1.6, 2.0, or 2.4	10, 15, or 25	0.25
M3D-Floc	1.6 or 2.4	10 or 15	0.25-0.5

Some common model parameters for all simulations are chosen based on sensitivity tests and existing literature (van der Wegen and Roelvink, 2008; van der Wegen

et al, 2008; Zhou et al, 2014b; Guo et al, 2015b), including, e.g. hydrodynamic time step (2 min), critical shear stress for erosion (0.5 Pa), horizontal eddy viscosity (1 m^2/s), horizontal eddy diffusivity (10 m^2/s), Chézy frictional coefficient (65 $m^{1/2}/s$), mud erosion parameter (10^{-4} $kg/m^2/s$), bulk density (500 kg/m^3) and morphological factor (200). The critical shear stress for deposition is set to a very large value (1000 Pa) following the concept of continuous deposition (Winterwerp, 2007). The settling velocity is set to 0.25 mm/s for most of the simulations, while it may vary from 0.25 mm/s to 0.5 mm/s when flocculation is considered in several runs.

3 Results

3.1 Morphological evolution

Starting from a uniformly sloping bed, the model predicts the formation and development of a fluvio-deltaic system (Figure 3) which is morphologically similar to natural systems such as the Fly River estuary and the Yangtze estuary (Figure 1). Near the estuary mouth, a number of distributary channels are developed cutting through the delta which is fan-shaped due to the diverging-converging bidirectional flow.

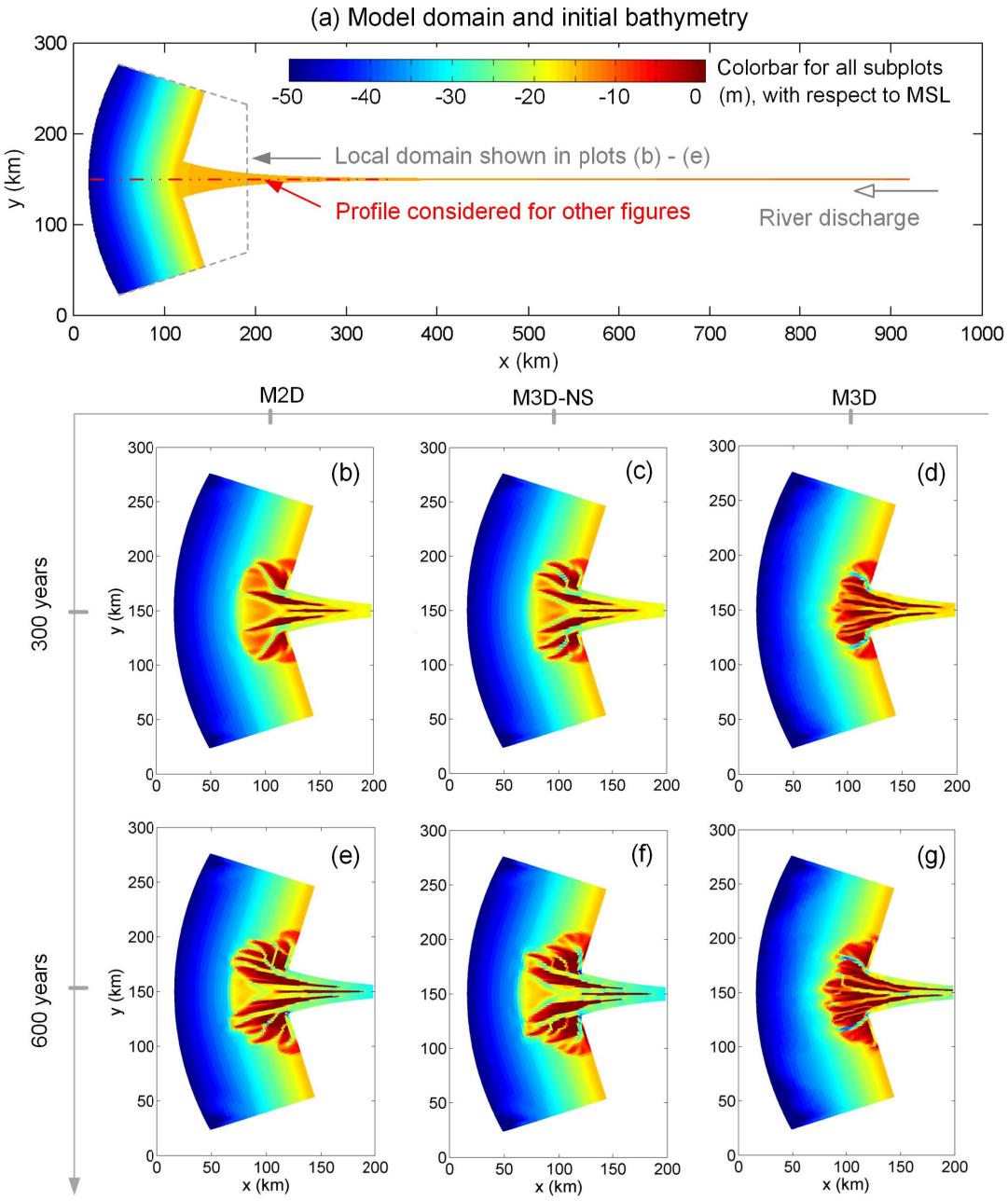

Figure 3: (a) Model domain and initial bathymetry, simulated bathymetries after 300 and 600 years when the model is run in (b, e) 2D and salinity is not considered, (c, f) 3D and salinity is not considered, (d, g) 3D and salinity is considered. All these runs are under the same tidal and fluvial conditions (TR = 2.4 m, Q = 15000 m^3/s). Note that the red dash-dot line in subplot (a) indicates the location of a profile for subsequent analyses and figures.

232 If salinity is not considered, the model produces comparable morphologies in 2D
233 or 3D modes after 600 years (Figure 3e-f). The major morphological difference lies

in the delta area with branching channels. In this region with large horizontal gradient in surface elevation, the secondary flow (e.g. transverse circulation) which can be captured by 3D models may play a role. Although there are some differences in terms of locally detailed bathymetries, the overall morphology characterized by the delta size and the channel-bar patterns does not differ much between the two cases (Figure 3e-f). However, a considerably different morphology is generated when salinity is considered. The delta size appears to be much smaller and the channels tend to be narrower (Figure 3e and g). More sediment tends to accumulate near the estuary mouth when salinity is included, leading to the formation of a more compact delta. The significant difference occurs where x-distance is smaller than approximately 200 km (where along-estuary salinity gradients are strongest), while the difference more close to river side is minor (i.e. $x >$200 km). Later, it will be shown that the region with $x <$200 km is a highly dynamic zone with the most baroclinic influence and the region with $x >$200 km is more controlled by the barotropic forcing. It should be noted that the x-distance value of transition can differ for various combinations of tidal and fluvial conditions and is determined by the relative strength of tidal and river discharge. A larger tidal range or a smaller fluvial discharge can result in a large x-distance value of transition, favouring a longer length of salt intrusion.

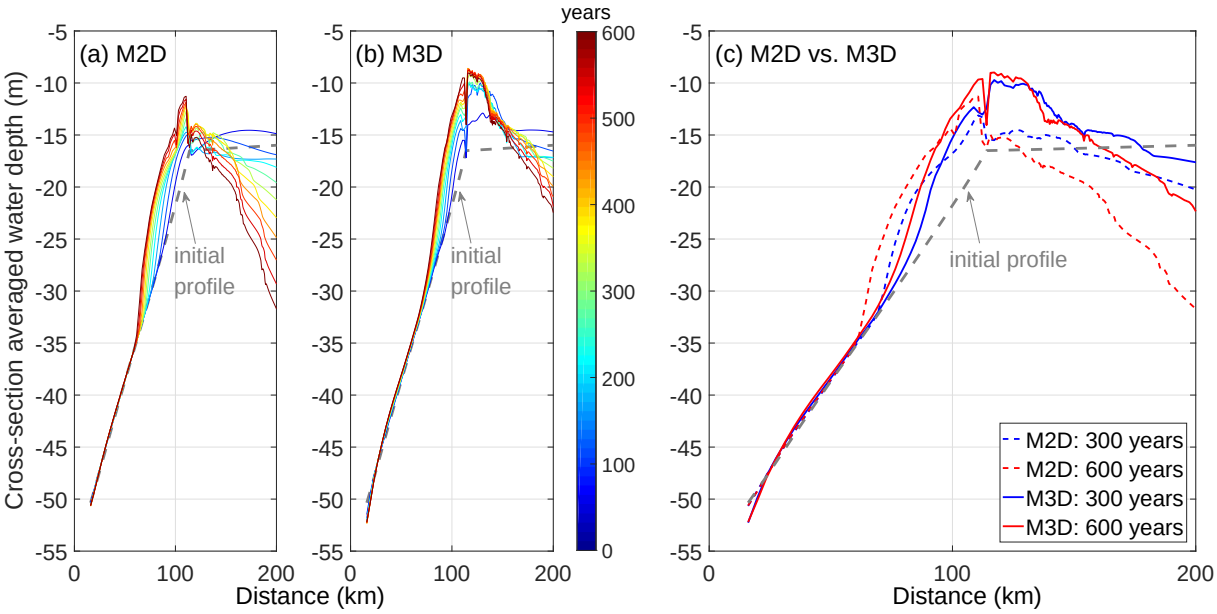

Figure 4: (a) and (b) Evolution of the cross-section averaged water depth along the estuary for the M2D, and the M3D cases, and (c) Comparison of M2D and M3D cases after 300 and 600 years. Note that the colour bar indicates time and the curves are plotted every 55 years. The corresponding 2D morphologies are shown in Figure 3b, d, e and g.

The morphodynamic evolution of the fluvio-deltaic system is characterised by a rapid development in the beginning (when the system is far from equilibrium) and a gradual adaptation toward a stable configuration in both M2D and M3D cases. It is noted that the overall resultant morphology in terms of channel-shoal distribution after 600 years does not differ too much compared to the one after 300 years (Figure 3), while the major difference lies in the size of the delta, the number and the depth of channels. This is also partially reflected by the evolution of the cross-section averaged water depth along the estuary (Figure 4a-b). Consistent with the morphological development shown in Figure 3, the delta develops approximately 5 km more seaward in the M2D case than in the M3D case (Figure 4c). At the estuary mouth (i.e. x-distance = 125 km), the cross-section averaged water depth is about 3 m higher in the M3D case than in the M2D case after 600 years and this value increases to more than 5 m further upstream of the estuary, indicating that inclusion of salinity favours landward sediment

transport and hence limits the growth of the delta.

3.2 Pattern formation of different cases

Pattern formations of all other sensitivity runs, with varying tidal ranges (TR), river discharges (Q) and settling velocities when flocculation is included (w_s), are compared in Figure 5. The effect of salinity is included in all M3D simulations and not in M2D ones, because the M3D-NS neutral simulation without salinity produces an overall consistent morphology as the M2D case (as demonstrated in Figure 3). In order to save computational cost, the M2D runs are considered instead of the 3D runs without salinity. Subplots (a)-(j) focus on the influence of tidal range and river discharge under both 2D and 3D modes, while (k)-(m) focus on the effect of flocculation. The delta area and the maximum number of channels are calculated for more detailed quantitative evidence. By calculating the elevation gradient between adjacent grid cells, the seaward boundary of delta can be distinguished and hence the delta area can be estimated. The maximum number of channels on the delta is counted using different sections for different cases (because the growth of the delta is different, see Figure 5).

The relative strength of fluvial and tidal discharges is the key factor governing the estuarine pattern formation. Model results indicate that larger river discharges (Q_R) result in more pronounced delta formation (for both M2D and M3D runs) because of the stronger erosion of sediment from the upstream river bed (Figure 5), which was also reported in Zhou et al (2014b) and Guo et al (2015b). The distributary channels appear to be deeper when Q is larger, due to the river-enhanced ebb current. Besides, more channels and detached mouth bars are formed under larger river discharges (see, particularly, Figure 5e and j). As can be seen in Figure 6d, the maximum number of channels generated in the M2D case is 10 when Q is 1.0 $\times 10^4$ m^3/s and doubles when Q is 2.5$\times 10^4$ m^3/s. Accordingly, the delta area in the M2D case increases from approximately 4500 km^2 to 7300 km^2 when Q increases from 1.0 $\times 10^4$ m^3/s to 2.5$\times 10^4$

291 m^3/s (Figure 6a). Finally, it is worth noting that the delta morphology displays a more
292 fluvial nature characterized by a bird-foot shape as discussed in Galloway (1975) given
293 larger fluvial discharge.

294 When Q is fixed, an increasing TR tends to result in a larger delta, more and wider
295 distributary channels (Figure 5a, b and d). The maximum number of channels in-
296 creases from 6 to 13 when tidal range increases from 1.6 m to 2.4 m (Figure 6d). The
297 delta area is approximately doubled when tidal range increases from 1.6 m to 2.4 m
298 (Figure 6a). Since the model considers a long river whose boundary is hardly affected
299 by the tide, the amount of supplied sediment eroded from the upstream river bed for all
300 cases is almost identical given the same discharge. The upstream river-bed sediment
301 is mostly redistributed within the model domain except for a small portion that is carried
302 out to the outer sea. The tidal forcing acts as a key factor to redistribute the sediment
303 and the channel-shoal patterns in the delta system are more developed provided larger
304 tidal energy.

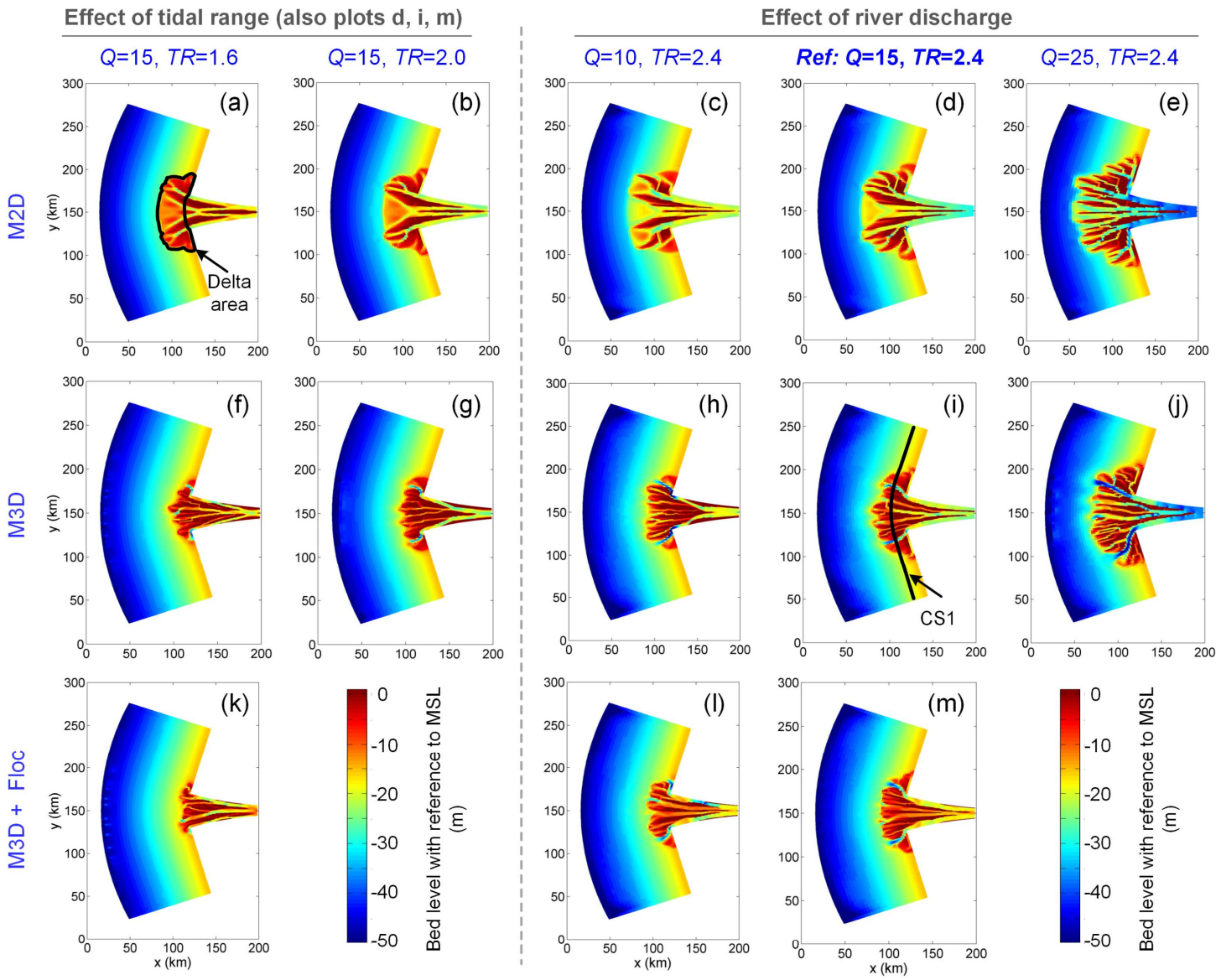

Figure 5: Resultant estuarine morphologies (the area indicated by the dashed box in Figure 3a) after 600 years under different conditions by varying tidal ranges, river discharges, sediment settling velocities and simulation modes (Table 1). The black curves in subplot (a) and (i) indicate the delta area and cross-section considered in subsequent analyses.

Compared to the M2D cases, the inclusion of salinity in the M3D model is found to considerably alter the resultant delta morphologies after 600 years (Figure 5f-j). The delta area generated in the M3D cases appears to be smaller than that in the M2D cases. When the tidal range is small (e.g., TR = 1.6 m), the delta area of the M2D case is approximately doubled compared to that of the M3D case. The delta area tends to be comparable between the M2D and M3D cases when tidal range increases to 2.4 m. Similarly, the delta area of the M3D case appears to approach the M2D case provided an increase in river discharge (with a fixed tidal range), because the influence of salinity is less profound if the river discharge is comparably large so that the impact of tide tends to be more seaward and relatively small. To better illustrate this behaviour, Figure 6b and 6c show variations of the ratio of delta area between the M3D and M2D cases (indicated by $A_{3D/2D}$) with tidal range and river discharge, respectively. Increasing either tidal range or river discharge (while fixing the other) tends to produce a more comparable delta area between the M2D and M3D cases, indicating that the combination of tidal and fluvial forcing plays a key role in salinity stratification and its associated flow dynamics. The dominance of either tidal or fluvial forcing results in less stratification and hence a more comparable delta area between the M2D and M3D cases (Figure 6a-c), so that the depth-averaged 2D mode may be applicable under such conditions.

Apart from the impact on the generated bulk delta area, salinity gradients can also significantly affect the detailed channel-shoal morphology on the delta. In particular, channels generated in the M3D cases appear to be narrower due to baroclinic effects. Accordingly, the number of channels dissecting the delta is more in the M3D cases than that in the M2D cases (Figure 6d). An increase in tidal range or river discharge results in the formation of more channels. The effect of river discharge on channel formation is particularly evident. When the river discharge increases to 2.5 $\times$ 10^4 m^3/s, the number of channels generated on the delta reaches 20 and 24 in the M2D and

M3D cases, respectively.

It is worth noting that the effect of fine-sediment flocculation (represented by a varying settling velocity w_s) on the morphodynamic development is considerable (Figure 5k-m). Using the simple formulation linking settling velocity to salinity (Deltares, 2014), the inclusion of flocculation effects results in a smaller delta area and the formation of less channels on the delta (curves marked with crosses in Figure 6a and d). The delta is hardly present for the case shown in Figure 5k. Because of the enhanced settling, the suspended river-bed fine sediment can deposit more rapidly near the estuary mouth before being flushed outside of the estuary, which can be the reason for the smaller delta generated. Overall, it appears that the spatial and temporal variation of settling velocity greatly affects the resultant morphology, which has been commonly overlooked owing to our limited understanding of the flocculation process.

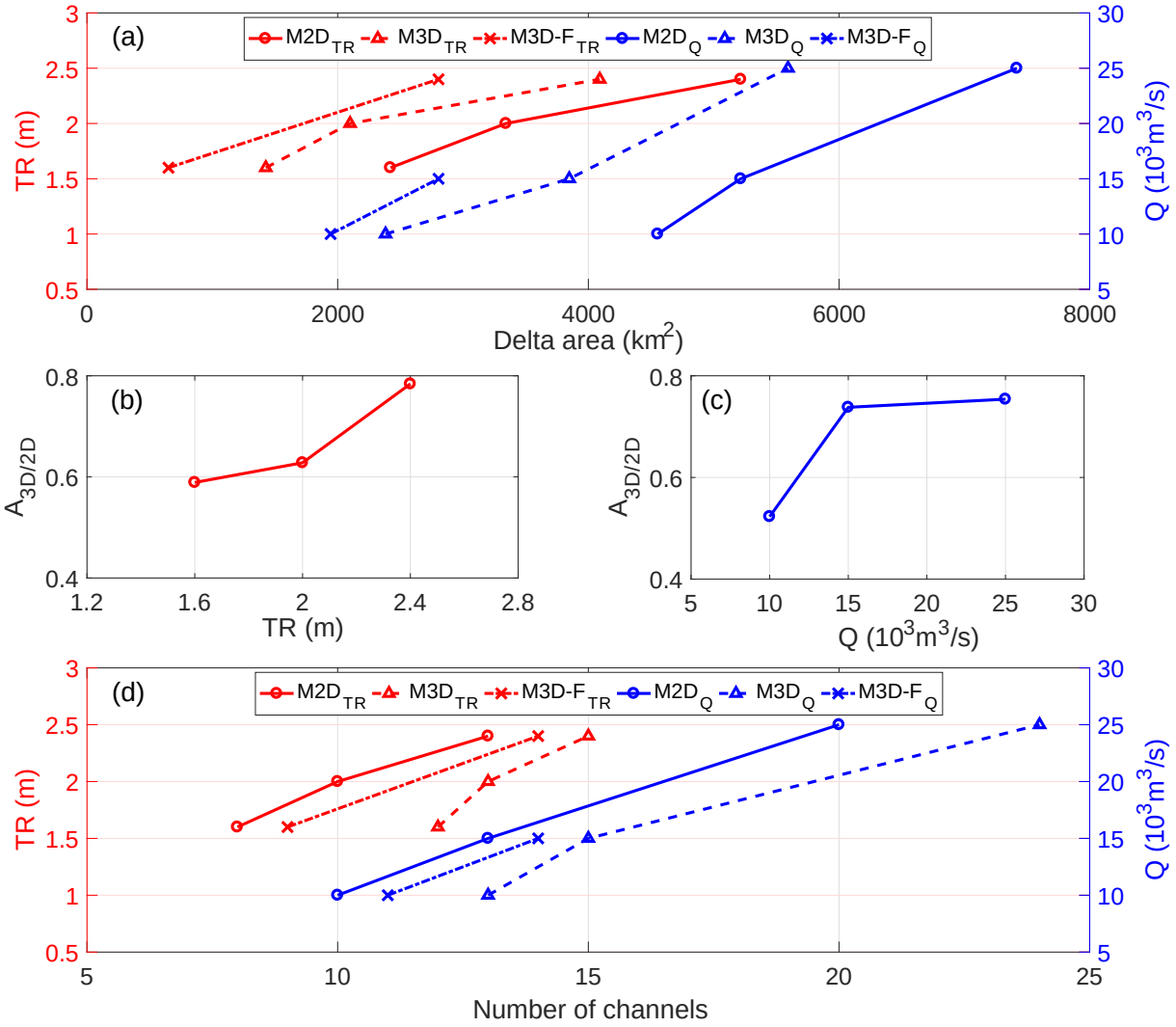

Figure 6: (a) The change of delta area as shown in Figure 5a with tidal range (TR) and river discharge (Q), (b) and (c) show the variations of the ratio of delta area between the M3D and M2D cases (indicated by $A_{3D/2D}$) with tidal range and river discharge, respectively, and (d) The change of number of channels with tidal range (TR) and river discharge (Q). The reference tidal range and river discharge are respectively 2.4 m and 1.5×10^4 m^3/s. The corresponding fluvio-deltaic morphologies are shown in Figure 5.

3.3 Hydrodynamics and stratification

Hydrodynamic results are quite useful to provide insight into the morphological differences resulted from the above different model settings. In this section, we focus on the HS2D and HS3D simulations (see Table 1) in which morphodynamic updating is not switched on, so that it is less computationally expensive. Therefore, a fixed linearly

sloping bathymetry is used for all the simulations. To simplify the analysis, we only consider the runs with a fixed river discharge (Q_R = 15000 m^3/s), while vary the tidal range (from TR = 1.6 to 3.2 m) to reflect the relative strength of fluvial and tidal forcing.

The salinity stratification is most evident near the central estuary mouth where saline and fresh water interacts significantly. The simulated salinity profiles at an instant during flood and ebb near the central estuary mouth are shown in Figure 7a-b. The vertically sheared along-estuary velocity results in stratification which can suppress turbulence. The stratification during ebb is more pronounced than that during flood when turbulence and vertical mixing are stronger, and hence sediment tends to be more confined near the bottom during ebb (Ralston, 2005; Ralston et al, 2013). During flood, the enhanced mixing reinforcing bottom turbulence promotes the entrainment of bottom sediment into the water column, favouring landward sediment transport. This intratidal asymmetry of stratification has been found to play a profound role in sediment pumping in estuaries, contributing considerably to the formation of the estuary turbidity maximum (Scully and Friedrichs, 2007; Gong et al, 2014; Geyer and MacCready, 2014). The relative strength of the tidal and fluvial forcing highly affects the stratification. Figure 7c-d shows the simulated salinity profiles near the central estuary mouth under tidal ranges of 1.6 and 3.2 m. The vertical distribution of salinity exhibits stronger stratification if TR is small (Figure 7c). When tidal forcing is comparatively strong, the riverine fresh water and oceanic saline water can be well mixed leading to a relatively uniform vertical distribution of salinity (Figure 7d).

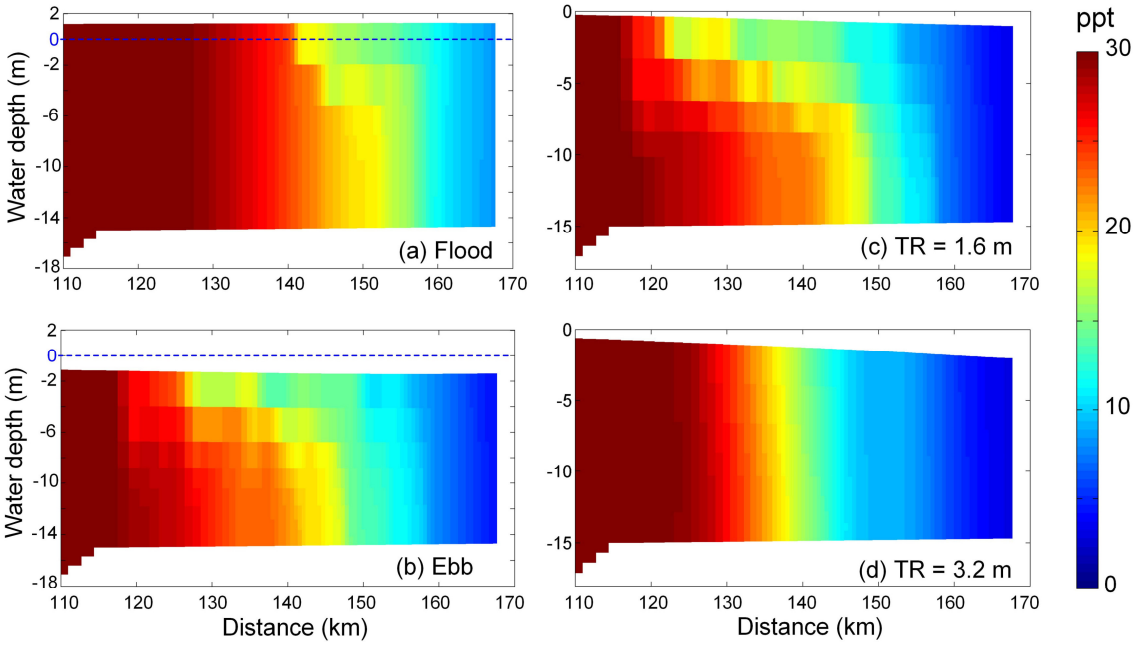

Figure 7: (a-b) Examples of simulated salinity profiles during flood phase close to high water level (HWL) and ebb phase close to low water level (LWL), H3D simulations under Q = 15000 m^3/s and TR = 1.6 m, (c-d) Examples of simulated salinity profiles under tidal ranges of 1.6 and 3.2 m at the same time instant during ebb close to MSL (H3D simulations under Q = 15000 m^3/s). Note the location of profile is indicated by the red dash-dot line in Figure 3a.

A well-established index indicating the stability of a stratified water column is the dimensionless gradient Richardson number (Richardson, 1920; Uncles and Stephens, 1996; Savenije, 2012):

$$R_i = \frac{-g\dfrac{\partial \rho}{\partial z}}{\rho\left[\left(\dfrac{\partial u}{\partial z}\right)^2 + \left(\dfrac{\partial v}{\partial z}\right)^2\right]} \tag{2}$$

where, ρ is the water density, g is the gravity acceleration constant, z is the vertical coordinate, u and v are the velocities in the x and y directions, respectively. Several classic studies suggest the existence of a critical R_i value of 0.25 above which a stable salinity stratification tends to occur, while below which the stratification tends to be unstable and hence tidal mixing is likely to occur (e.g. Taylor, 1931; Goldstein, 1931;

Uncles and Stephens, 1996).

Figure 8 shows the temporal variation of the cross-section averaged surface and bottom gradient Richardson number on a cross-channel section in the delta (indicated by CS1 in Figure 5i). Consistent with Figure 7, salinity stratification at the surface appears to be larger than that at the bottom where R_i is smaller than 0.03 (Figure 8b). The relative strength of tidal and fluvial forcing considerably affects the condition of tidal mixing. A smaller tidal range (TR = 1.6 m) tends to result in larger values of R_i and hence more pronounced stratification for the cases considered, which is also reflected by the salinity profile (Figure 7c-d). Tidal mixing or stratification is also highly dependent on the flood and ebb tidal phases. Consistent with Figure 7a-b, stronger salinity stratification characterised by larger values of R_i tends to occur during the ebb phase than the flood phase. Existing studies suggest that bathymetry plays an important role on tidal mixing (Lacy, 2003; Ralston, 2005; Geyer and MacCready, 2014). For example, Lacy (2003) observed that complex bathymetry in northern San Francisco Bay can strengthen stratification during flood tides due to a lateral baroclinic pressure gradient. Numerical results obtained using an initial and evolved bathymetry show that the value of R_i appears to be larger when the more complex bathymetry of channel-shoal patterns is considered (Figure 8a), indicating that morphodynamic evolution can considerably affect salinity stratification. Finally, it is worth mentioning that tidal mixing and stratification processes are driven by multiple factors (e.g. wind, tide, river discharge, bathymetry) and it becomes even more complex when human intervention is strong as e.g. the Yangtze Estuary (Shi, 2010; Shi and Lu, 2011) or the Pearl River Delta (Zhang et al, 2018).

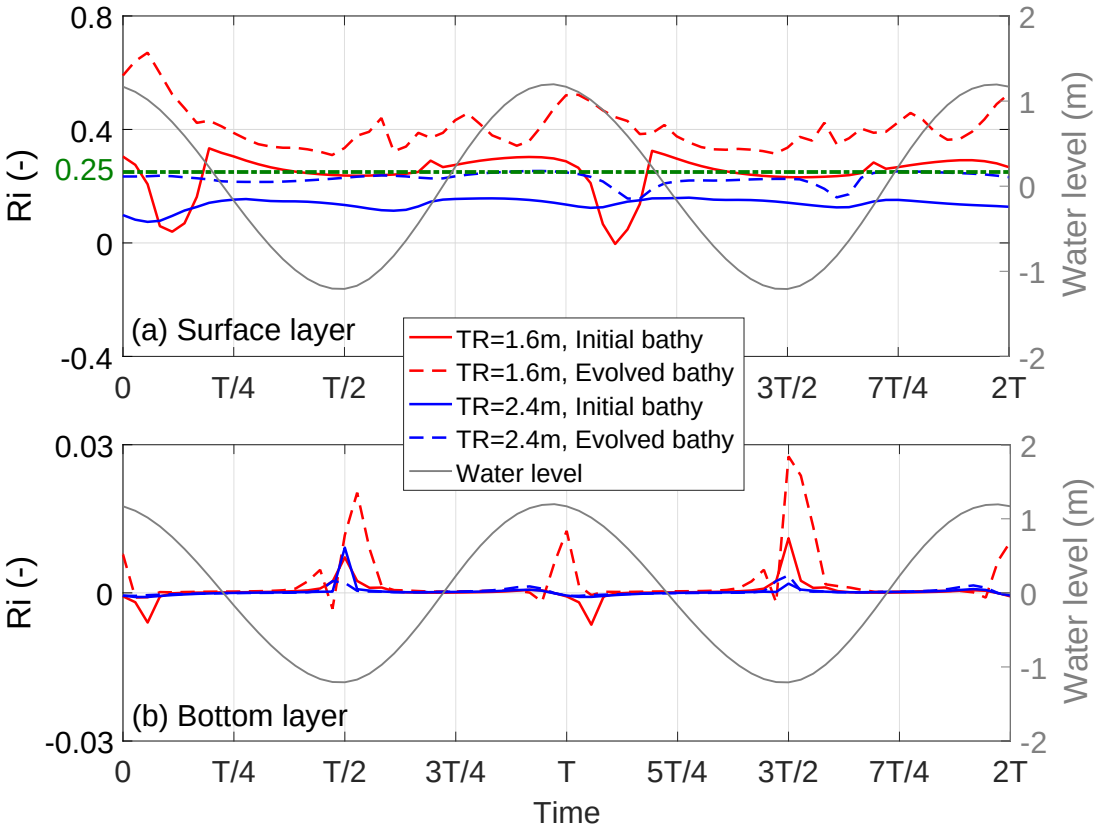

Figure 8: The variation of the cross-section averaged surface and bottom gradient Richardson number on a cross-channel section in the middle of the delta shown in Figure 5i. Four cases are considered by varying the tidal range (TR = 1.6 m and 2.4 m) and the bathymetry ('Initial bathy' indicates the initial smooth bathymetry shown in Figure 3a, and 'Evolved bathy' indicates the evolved bathymetry with channel-shoal patterns shown in Figure 3g), under the same fluvial discharge (Q = 15000 m^3/s).

The condition of salinity stratification is closely linked to suspended sediment concentration and fine sediment transport. The along-channel and vertical distribution of suspended sediment concentration (SSC) under increasing tidal ranges is shown in Figure 9a-c. Noticeably, a high SSC zone comparable to an estuarine turbidity maximum (ETM) is formed within the inner estuary mouth. A larger TR results in a more seaward maximum SSC point (e.g. the maximum SSC point is located at about 260 km for the case of TR = 1.6 m while at about 200 km for TR = 3.2 m). This, at first glance, seems to be inconsistent with existing studies (e.g. van Maren et al, 2015). Through a detailed scrutiny, it was found that the SSC distribution highly depends on the spa-

tial distribution of flow velocities (and hence bed shear stresses). Given a larger tidal range, the maximum flow velocity and bed shear stress shifted in the down-estuary direction, resulting in the corresponding shifting of the maximum SSC point. However, the relatively high SSC zone (e.g., larger than 0.5 kg/m^3) in fact becomes larger with a larger tidal range. Therefore, in terms of the ETM zone, it indeed moves at the up-estuary direction because of the more landward coverage of large flow velocities. It should be noticed that a down-estuary shifting of the ETM zone is also possible under certain circumstances. For example, Grasso et al (2018) demonstrated that the down-estuary shifting of the ETM zone may occur provided a sufficiently large TR that can reduce the up-estuary density-driven baroclinic circulation (by increasing the mixing and reducing the stratification), but not large enough to enhance the tidal pumping mechanism. Recently, Grasso and Le Hir (2019) further found that the morphology can affect the stratification and the ETM zone may be mainly related to TR without the contribution of baroclinic circulation when the estuary is very shallow.

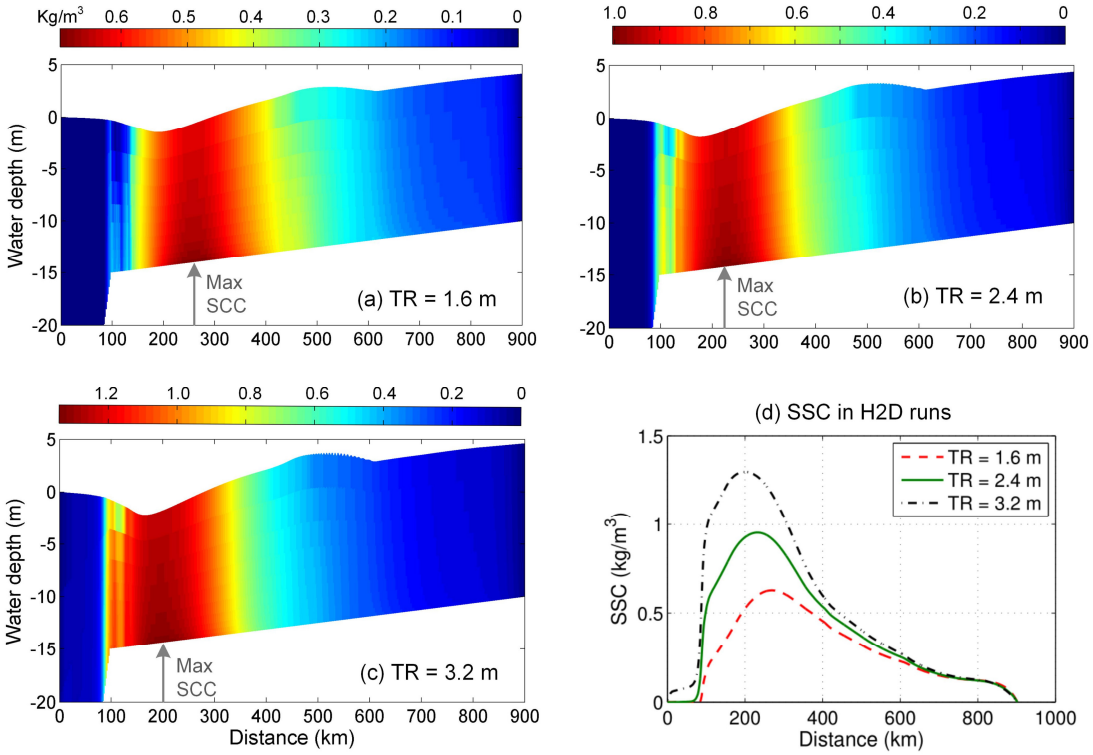

Figure 9: Examples of simulated suspended sediment concentration (SSC) profiles under increasing tidal ranges (1.6-3.2 m) at the same time instant during ebb in H3D simulations (a-c), and in H2D simulations (d). Other settings are the same: Q = 15000 m^3/s and w_s = 0.25 mm/s. Note the location of the profile is indicated by the red dash-dot line in Figure 3a.

Besides, the magnitude of the maximum SSC is also larger for larger TR, because more energy is supplied leading to more sediment suspension. For example, the maximum SSC reaches about 0.65 kg/m^3 for TR = 1.6 m while about 1.25 kg/m^3 for TR = 3.2 m. The longitudinal distribution of SSC is also calculated using 2D models and shown in Figure 9d. The 2D result is highly consistent with the 3D result in terms of both the location and magnitude of the maximum SSC. However, since the 2D simulation is not able to provide the vertical distribution of SSC which tends to be higher near the bottom and lower near the surface (elaborated below), it lacks an important aspect for the morphological evolution.

The residual velocity is often used to provide insight for morphodynamic indications. Figure 10 shows the residual velocity profiles near the estuary mouth under tidal

ranges of 1.6 m and 3.2 m. When TR is small, the river influence is relatively large and hence the effect of salinity is more evident leading to the formation of strong salinity stratification and salt wedge (Figure 7). This baroclinic effect in turn drives the landward residual velocity near the bottom (Figure 10a). The residual velocity near the free water surface is seaward, but it does not contribute as much to the sediment transport as near the bottom because of the associated lower SSC (Figure 9). In fact, this phenomena of different directional residual velocities at different levels of water depth has also been reported by Gong et al (2014) through extensive field measurement in the Pearl River Complex, China. When TR is large, this phenomena is less evident, because the vertical mixing is enhanced resulting in weaker stratification. Therefore, the residual velocity tends to be seaward throughout the water column (Figure 10b). It is worthwhile to note that the residual velocity throughout the water column can also be seaward when the relative strength of fluvial forcing is considerably large so that the barotropic effect dominates over the baroclinic effect.

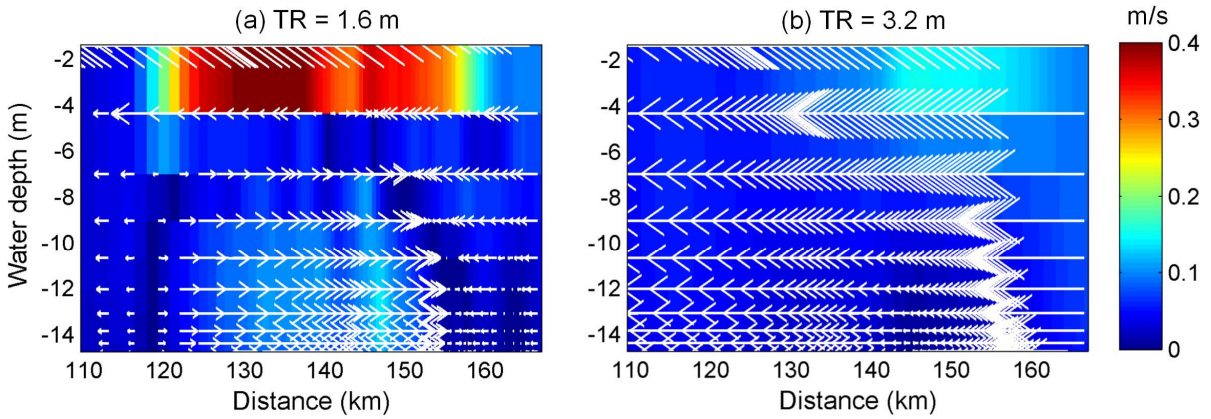

Figure 10: Examples of residual longitudinal velocity profiles under tidal ranges of 1.6 and 3.2 m (H3D simulations, color indicates the magnitude of residual velocities). Other settings are the same: Q = 15000 m^3/s and w_s = 0.25 mm/s. Note the location of profile is indicated by the red dash-dot line in Figure 3a.

A comparison of horizontal residual velocity and sediment transport is made between H2D and H3D simulations near the estuary mouth (Figure 11). Under 2D mode, the calculated residual velocity tends to be seaward, leading to a seaward residual

sediment transport (Figure 11a,c). This is primarily due to the river enhanced ebb dominance favoring the seaward residuals. However, both the depth-averaged residual velocity and depth-averaged sediment transport are significantly different under the 3D mode. The residual velocities in different locations in 3D are not smoothly aligned as in the 2D case. Although the residual velocities show an overall seaward direction, their local directions can differ considerably with even the presence of small circulations. It is also interesting to notice that the residual sediment transport in 3D does not necessarily show a direction consistent with the residual velocity (Figure 11b,d). In fact, the direction of the residual sediment transport opposes the residual velocity in the reach from 140 to 155 km. This seems to be counter-intuitive at the first sight, but it is actually understandable because the SSC near the bottom is much larger than near the surface. Although the seaward velocities near the surface may be large resulting in an overall seaward residual, they do not contribute much seaward sediment transport due to the low SSC near the surface. On the other hand, the landward velocities induced by salinity gradients near the bottom are quite effective to transport sediment landward because of the high SSC near the bottom. The different directions between the residual velocity and sediment transport in 3D mode are therefore understandable.

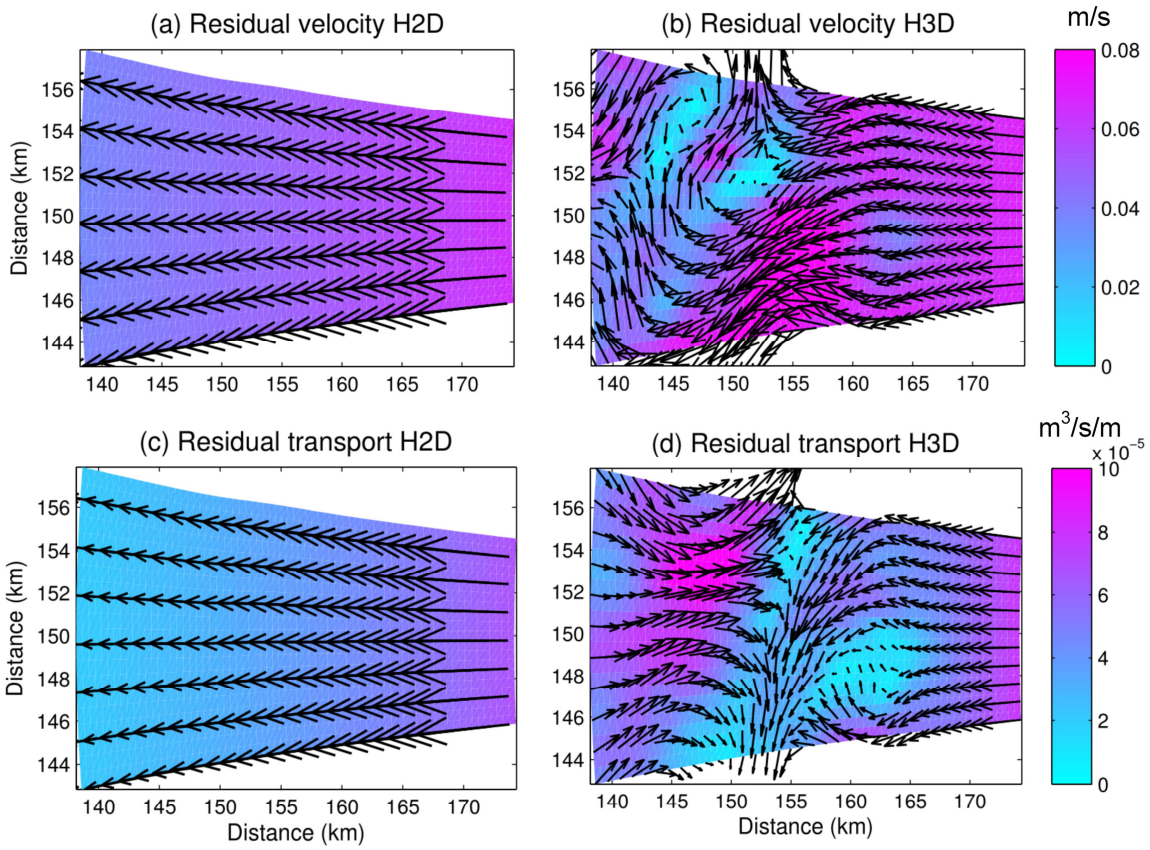

Figure 11: The horizontal depth-averaged residual velocity and depth-averaged sediment transport near the estuary mouth calculated over an entire tidal cycle based on the initial bathymetry, simulated using both H2D and H3D models under the same hydrodynamic conditions (TR = 1.6 m, Q = 15000 m^3/s). Color indicates the magnitude of residual velocity or residual transport.

4 Discussion

Estuarine salinity gradients and associated baroclinic effects have been widely explored (Geyer and MacCready, 2014), with numerous studies focusing on baroclinicity induced estuarine circulation of flow and sediment, while research on direct morphological predictions is still limited (Dalrymple and Choi, 2007; Olabarrieta et al, 2018). Although debates still exist on the coupling of multiple-scale processes and the potential cascade effects of numerical errors, the use of long-term simulation models (with certain assumptions and limited processes) indeed provides some insight into the

mechanisms underlying the morphological evolution of estuarine systems. Because of the high computational cost required, direct long-term 3D morphodynamic simulations with salinity included are seldom performed. Using a high-performance cluster, this study is among the first to demonstrate the effect of salinity gradients on the long-term estuarine morphodynamics with a focus on fluvio-deltaic systems.

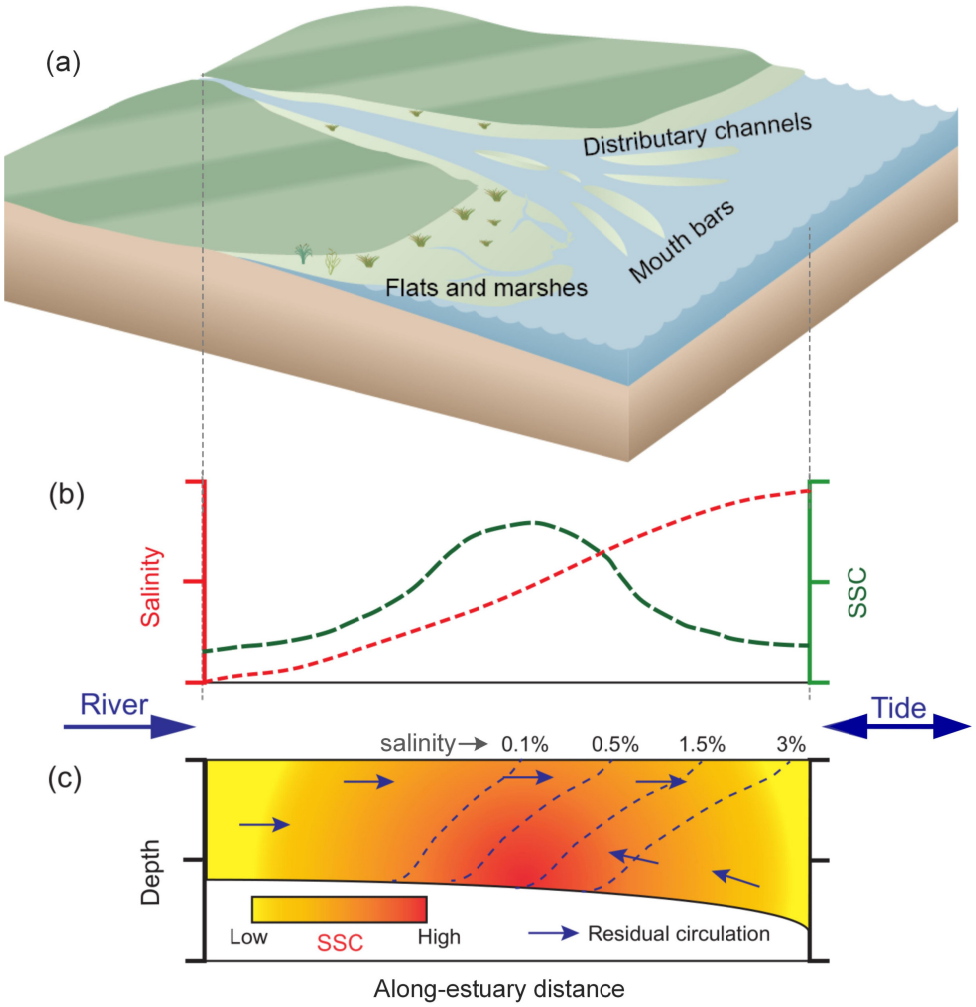

Figure 12: A conceptual diagram elaborating the estuarine hydrodynamic processes and the associated morphodynamic indications. Subplots (b) and (c) are re-drawn following Dalrymple and Choi (2007).

Compared to the results of the 2D simulations without salinity, the inclusion of salinity in the 3D model is found to considerably alter the resultant morphologies after 600 years (Figure 5). The resultant fan-shaped river-mouth delta expands less far sea-

wards and is cut through by more and narrower channels when the effect of salinity is included. Meanwhile, the growth of the delta appears to be limited and the sediment tends to be trapped near the estuary mouth, which is in agreement with the finding of Olabarrieta et al (2018) on the inner estuary part. The underlying mechanisms have been briefly summarized in Figure 12. By analysing the vertical structure of salinity and residual velocity near the estuary mouth, it is found that saltier water near the estuary mouth flows landward near the bottom while fresher water flows seaward near the surface (estuarine circulation). Since the suspended sediment concentration is higher near the bottom and decreases towards the water surface, the net effect of salinity favors landward sediment transport and hence limits the growth of the delta.

The long-term morphological response to baroclinic effects may be considerable depending on the local environmental setting. Figure 13 shows the evolution of tidal flat area and volume of the fluvio-deltaic region shown in Figure 3a (indicated by the dashed line), with corresponding morphologies shown in Figure 5. Tidal flat is defined as the area between the high and low water levels. The M3D cases (represented by solid lines, Figure 13) are generally characterised by more rapid development of intertidal areas than that of the M2D cases (dashed lines). For instance, it takes approximately 50 years before tidal flats to develop in the M3D cases, while 100-200 years are needed in the M2D cases. Besides, the M3D cases generally produce larger tidal flat areas and volumes than that of the M2D cases, although the resultant delta areas are larger in the M2D cases than that in the M3D cases (Figure 6a). Therefore, the inclusion of salinity favours the formation of intertidal area.

The relative strength between the tidal and fluvial forcing appears to be particularly important. Given a relatively large tidal but a small fluvial forcing (e.g. TR = 2.4 m and Q = 10000 m^3/s), the difference in tidal flat area and volume after 600 years between the 2D and 3D simulations tends to be most pronounced. When both the tidal and fluvial forcing are large (e.g. TR = 2.4 m and Q = 25000 m^3/s), the formation of tidal flats

after 600 years appears to be comparable between the 2D and 3D simulations. For intermediate flow conditions and tidal ranges there are multiple combinations of flow and tidal range that lead to very similar areas and volumes of tidal flat (the green, blue and red solid lines in Figure 13) in the M3D simulations. However, a further reduction in tidal range then produces a distinctly smaller area of tidal flat with a commensurately smaller volume (the dark solid line). This suggests that there are a range of flow and tidal range conditions that can establish an intermediate state between the two states defined by high and low flow/tide conditions. More curiously, the results of M3D-Floc cases for low tidal range conditions are similar to the 2D rather than the 3D simulations.

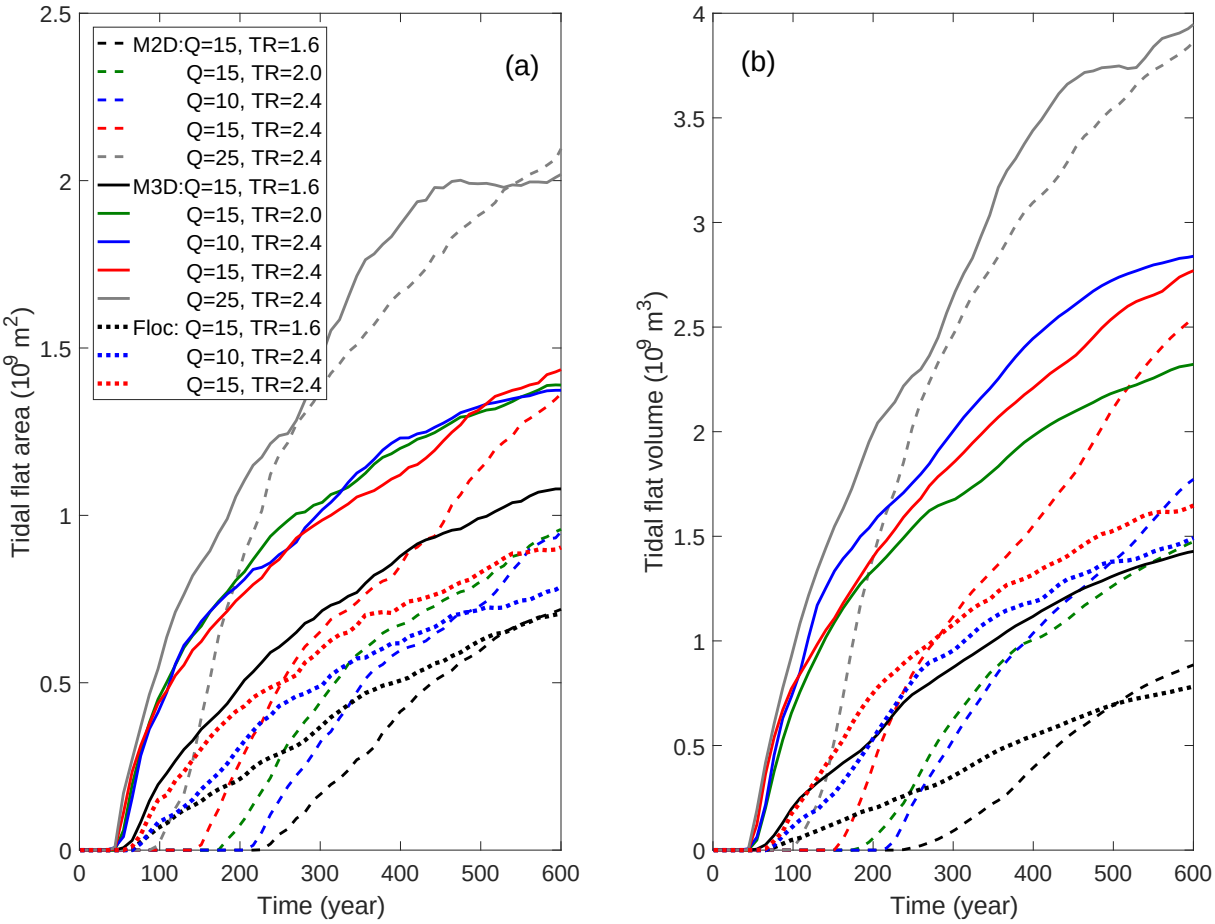

Figure 13: Evolution of tidal flat area and volume close to the estuary mouth as indicated by the dashed line shown in Figure 3a. The corresponding fluvio-deltaic morphologies are shown in Figure 5. The units of tidal range (TR) and river discharge (Q) are m and 10^3 m^3/s, respectively.

521 It seems that there exists a critical ratio between tidal and fluvial forcing that de-
522 termines the direction of net sediment transport. If the river discharge is dominant
523 compared to the tidal discharge, the strong ebb-directional barotropic flow can over-
524 come the baroclinic effect and flush the sediment away seaward. If the river discharge
525 is relatively large (but not excessively so), the landward sediment transport induced by
526 salinity may dominate over the river-enhanced ebb-directional transport, resulting in a
527 net landward transport. If the river forcing is comparatively small, the estuary can be
528 well mixed and hence the effect of salinity gradients is small. Therefore, the net sed-
529 iment transport is highly determined by this delicate balance between the baroclinic
530 effects favouring landward transport and the enhanced barotropic flushing favouring
531 seaward transport. This bears important implications for a tidal river with strong sea-
532 sonal variations in discharge conditions (Gong et al, 2014).

533 It is also noticed that sediment type and the associated transport modes play a
534 significant role on the pattern formation of fluvio-delta morphology. Fine cohesive sed-
535 iment, as normally observed in estuarine environments, differs significantly from its
536 non-cohesive counterpart in terms of both physical and electrochemical properties.
537 Cohesive sediment is commonly transported in the water column as suspended load
538 which lags behind hydrodynamic forcing to some extent and can be highly affected by
539 the baroclinic effects induced by a salinity gradient. On the one hand, salinity gradients
540 can enhance flocculation favouring sediment settling and hence limiting the growth
541 of tidal flats on the delta as seen in Figure 13, and on the other hand, the associ-
542 ated baroclinic effects can modify the flow structure and hence affect suspended sed-
543 iment transport. Depending on the grain size and hydrodynamic conditions, the non-
544 cohesive sediment can be transported as both bedload and suspended load. Coarser
545 non-cohesive sediment normally responds more rapidly to hydrodynamic conditions
546 (Dronkers, 1986). These different physical properties and dynamic characteristics of
547 cohesive and non-cohesive sediment result in distinctive estuarine morphologies even

under 2D mode (Edmonds and Slingerland, 2010). As shown in Figure 14, the sandy setting, well-mixed 2D conditions as considered in Guo et al (2015b) leads to more complex patterns which are characterized by the presence of scattered sand bars and more frequent branching and braided channels. Less and straighter channels are produced in the muddy setting of the present 3D study, which appear to be morphologically comparable to natural systems (Figure 1). It is worth noting that the 3D baroclinic effects on estuarine morphodynamics cannot be well simulated using the sandy setting as considered in previous studies (e.g. Zhou et al, 2014a; Guo et al, 2015b), particularly when the bedload transport mode is assumed. This is still a research area awaiting more investigation.

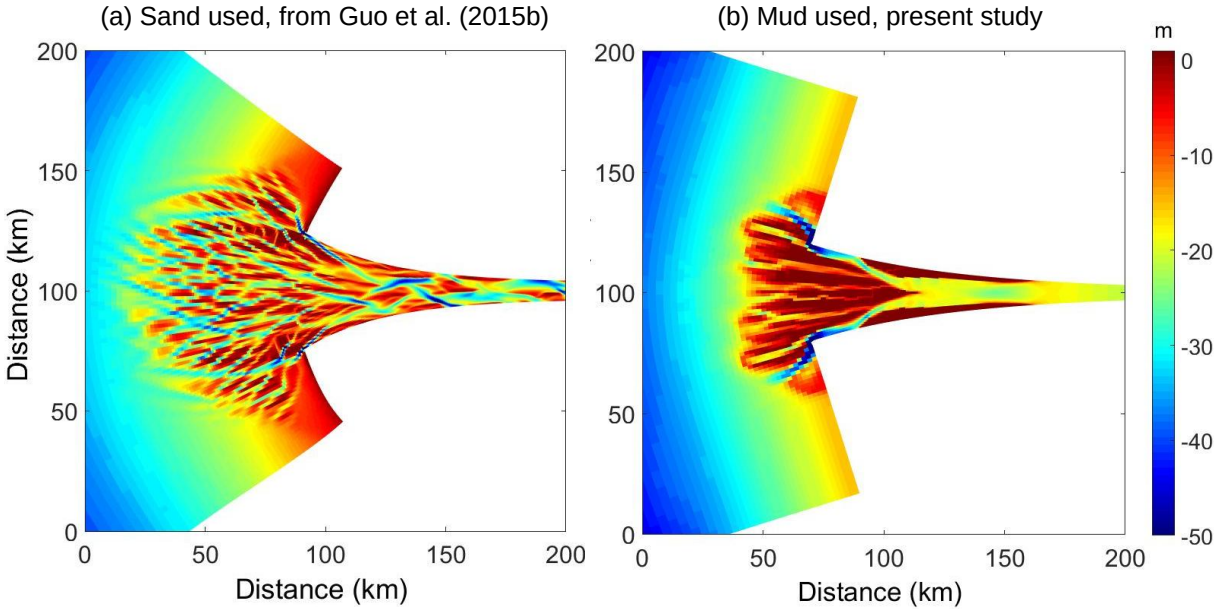

Figure 14: A comparison of resultant morphologies of two studies after 500 years under the same tidal range and river discharge (TR = 2.4 m, Q = 10000 m^3/s): (a) 2D model with sand sediment by Guo et al (2015b) in which the sediment transport formula of Engelund and Hansen (1967) was used, and (b) 3D model with mud sediment in the present study. Note that the exact model domain is slightly different between the two studies, but the model dimension is similar.

Although the influence of salinity on estuarine morphology may be insignificant over shorter periods, its effect can accumulate over time and result in a non-negligible effect in the long run. Present morphodynamic models neglecting salinity may overestimate

561 the size of the delta. Therefore, neglecting salinity in long-term estuarine morphody-
562 namic simulations requires careful justification, particularly when the estuarine environ-
563 ment is characterized by the presence of fine sediment (favouring suspended transport
564 and flocculation) and relatively large river discharges. More effort is needed to quanti-
565 tatively characterise the link between tidal and fluvial discharges and the baroclinicity-
566 influenced morphology. Additionally, the effects of the neglected processes, such as
567 tidal asymmetry, multiple sediments, waves, spring-neap tidal cycles, fluvial sediment
568 supply and seasonally varying river discharges may also be important. For example,
569 a tidal asymmetry characterised by a shorter flood duration than the ebb (i.e. flood-
570 dominance) can lead to the infilling of the estuary which may be enhanced by the 3D
571 salinity-induced effect (Olabarrieta et al, 2018). On the other hand, a river discharge
572 can enhance ebb dominance favouring seaward sediment transport, and a seasonally
573 varying river discharge as observed in many natural systems can greatly change the
574 salinity structure and hence affect net sediment transport (Cai et al, 2014; Grasso et al,
575 2018). Sediment types, as briefly discussed along with Figure 14, play a significant role
576 on estuarine morphology. Estuaries are commonly characterised by mixed sediments
577 of various grain sizes which may respond differently to salinity structure and its asso-
578 ciated flow (Dronkers, 1986). Besides, the sorting behaviour of mixed sediments in
579 estuaries may be affected by including salinity (Zhou et al, 2015). To promote a better
580 understanding and facilitate the future prediction of the fluvial-deltaic morphodynamics,
581 further research awaits to address the detailed effects of these neglected processes.

582 5 Conclusions

583 The effects of salinity on the long-term morphodynamic evolution of a schematic fluvio-
584 deltaic system are investigated using a state-of-the-art morphodynamic model. Model
585 results suggest that the resultant fan-shaped river-mouth delta expands less far sea-

wards and is cut through by more and narrower channels when the effect of salinity is included. The growth of the delta appears to be limited and the sediment tends to be trapped near the estuary mouth, favouring the development of intertidal areas. The relative strength of fluvial and tidal discharges is the key factor determining the stratification condition and governing the estuarine morphologies. Simulations with a small tidal range and a comparatively large river discharge tend to result in larger values of the gradient Richardson number and hence more pronounced stratification. When either tidal and fluvial forcing is dominant, the general morphodynamic development after 600 years tends to be comparable between the 2D and 3D simulations as salinity stratification is weak. Sediment types and transport modes are also found to play a considerable role on long-term estuarine morphodynamic evolution, particularly when baroclinic effects are concerned. The channel-shoal patterns resulting from morphodynamic evolution can modify the condition of tidal mixing, showing a strong bathymetric control on salinity stratification. Overall, this study suggests that middle to long-term estuarine morphodynamic models (from decades to millennia) are likely to overestimate the growth of the delta and generate wider deltaic channels if salinity gradients between the ocean and the river are overlooked. Therefore, neglecting salinity in long-term estuarine morphodynamic simulations with fine sediment requires more careful justification.

Acknowledgements

This study is supported by the National Key Research and Development Program of China (Grant No. 2016YFC0401505), the National Natural Science Foundation of China (Grant Nos. 41606104, 51620105005), the Natural Science Foundation of Jiangsu Province (Grant No. BK20160862), and the Jiangsu Marine Science and Technology Innovation Programme (Grant No. HY2018-1).

References

Braat L, van Kessel T, Leuven JRFW, Kleinhans MG (2017) Effects of mud supply on large-scale estuary morphology and development over centuries to millennia. Earth Surface Dynamics 5(4):617–652, DOI: 10.5194/esurf-5-617-2017

Burchard H, Baumert H (1998) The formation of estuarine turbidity maxima due to density effects in the salt wedge. a hydrodynamic process study. Journal of Physical Oceanography 28(2):309–321

Cai H, Savenije HHG, Toffolon M (2014) Linking the river to the estuary: influence of river discharge on tidal damping. Hydrology and Earth System Sciences 18(1):287–304, DOI: 10.5194/hess-18-287-2014

Coco G, Zhou Z, van Maanen B, Olabarrieta M, Tinoco R, Townend I (2013) Morphodynamics of tidal networks: advances and challenges. Marine Geology 346:1–16, DOI: 10.1016/j.margeo.2013.08.005

Dalrymple RW, Choi K (2007) Morphologic and facies trends through the fluvial-marine transition in tide-dominated depositional systems: A schematic framework for environmental and sequence-stratigraphic interpretation. Earth-Science Reviews 81(3-4):135–174, DOI: 10.1016/j.earscirev.2006.10.002

Deltares (2014) Delft3d-flow user manual: Simulation of multi-dimensional hydrodynamic flows and transport phenomena, including sediments. Tech. rep., Deltares, Delft, The Netherlands, version: 3.15.34158

Dronkers J (1986) Tidal asymmetry and estuarine morphology. Netherlands Journal of Sea Research 20(2-3):117–131, DOI: 10.1016/0077-7579(86)90036-0

Edmonds DA, Slingerland RL (2010) Significant effect of sediment cohesion on delta

morphology. Nature Geoscience 3(2):105–109, DOI: 10.1038/ngeo730, identifier: ngeo730

Engelund F, Hansen E (1967) A monograph on sediment transport in alluvial streams, vol 33. Teknisk Forlag, Copenhagen, Denmark

Galloway WE (1975) Process framework for describing the morphologic and stratigraphic evolution of deltaic depositional systems. In: Broussard M (ed) Deltas: Models for exploration, Houston Geological Society, Houston, TX, pp 87–98

Ganju NK, Schoellhamer DH, Jaffe BE (2009) Hindcasting of decadal-timescale estuarine bathymetric change with a tidal-timescale model. Journal of Geophysical Research: Earth Surface 114(F4), DOI: 10.1029/2008JF001191

Geyer WR, MacCready P (2014) The estuarine circulation. Annual review of fluid mechanics 46:175–197, DOI: 10.1146/annurev-fluid-010313-141302

Goldstein S (1931) On the stability of superposed streams of fluids of different densities. Proceedings of the Royal Society of London Series A, Containing Papers of a Mathematical and Physical Character 132(820):524–548, URL http://www.jstor.org/stable/95675

Gong W, Shen J (2011) The response of salt intrusion to changes in river discharge and tidal mixing during the dry season in the modaomen estuary, china. Continental Shelf Research 31(7-8):769–788, DOI: 10.1016/j.csr.2011.01.011

Gong W, Jia L, Shen J, Liu JT (2014) Sediment transport in response to changes in river discharge and tidal mixing in a funnel-shaped micro-tidal estuary. Continental Shelf Research 76(2):89107, DOI: 10.1016/j.csr.2014.01.006

Grasso F, Le Hir P (2019) Influence of morphological changes on suspended sediment dynamics in a macrotidal estuary: diachronic analysis in the seine estuary (france)

from 1960 to 2010. Ocean Dynamics 69(1):83–100, DOI: 10.1007/s10236-018-1233-x

Grasso F, Verney R, Le Hir P, Thouvenin B, Schulz E, Kervella Y, Khojasteh Pour Fard I, Lemoine JP, Dumas F, Garnier V (2018) Suspended sediment dynamics in the macrotidal seine estuary (france): 1. numerical modeling of turbidity maximum dynamics. Journal of Geophysical Research: Oceans 123(1):558–577, DOI: 10.1002/2017JC013185

Guo L, van der Wegen M, Jay DA, Matte P, Wang ZB, Roelvink D, He Q (2015a) River-tide dynamics: Exploration of nonstationary and nonlinear tidal behavior in the Yangtze River estuary. Journal of Geophysical Research: Oceans 120(5):3499–3521, DOI: 10.1002/2014JC010491

Guo L, van der Wegen M, Roelvink DJA, Wang ZB, He Q (2015b) Long-term, process-based morphodynamic modeling of a fluvio-deltaic system, part i: The role of river discharge. Continental Shelf Research 109:95–111, DOI: 10.1016/j.csr.2015.09.002

Hibma A, De Vriend H, Stive M (2003a) Numerical modelling of shoal pattern formation in well-mixed elongated estuaries. Estuar Coast Shelf Sci 57(5–6):981–991, DOI: 10.1016/S0272-7714(03)00004-0

Hibma A, Schuttelaars H, Wang Z (2003b) Comparison of longitudinal equilibrium profiles of estuaries in idealized and process-based models. Ocean Dynamics 53(3):252–269, DOI: 10.1007/s10236-003-0046-7

Hibma A, Stive MJF, Wang ZB (2004) Estuarine morphodynamics. Coastal Engineering 51(8-9):765–778, DOI: 10.1016/j.coastaleng.2004.07.008

Huijts KMH, Schuttelaars HM, de Swart HE, Valle-Levinson A (2006) Lateral entrapment of sediment in tidal estuaries: An idealized model study. Journal of Geophysical Research 111(C12), DOI: 10.1029/2006JC003615

683 Lacy JR (2003) Interaction of lateral baroclinic forcing and turbulence in an estuary.
684 Journal of Geophysical Research 108(C3), DOI: 10.1029/2002JC001392

685 Lesser G, Roelvink J, van Kester J, Stelling G (2004) Development and validation
686 of a three-dimensional morphological model. Coastal Engineering 51(8-9):883–915,
687 DOI: 10.1016/j.coastaleng.2004.07.014

688 Manning AJ, Baugh JV, Spearman JR, Pidduck EL, Whitehouse RJS (2011) The set-
689 tling dynamics of flocculating mud-sand mixtures: Part 1empirical algorithm devel-
690 opment. Ocean Dynamics 61(2-3):311–350, DOI: 10.1007/s10236-011-0394-7

691 van Maren DS, Winterwerp JC, Vroom J (2015) Fine sediment transport into the hyper-
692 turbid lower ems river: the role of channel deepening and sediment-induced drag
693 reduction. Ocean Dynamics 65(4):589–605, DOI: 10.1007/s10236-015-0821-2

694 Monismith SG, Kimmerer W, Burau JR, Stacey MT (2002) Structure and flow-induced
695 variability of the subtidal salinity field in northern san francisco bay. Journal of Phys-
696 ical Oceanography 32(11):3003–3019

697 Murray AB (2003) Contrasting the goals, strategies, and predictions associated with
698 simplified numerical models and detailed simulations. In: Geophys. Monogr. Ser., vol
699 135, AGU, Washington, DC, pp 151–165, URL http://dx.doi.org/10.1029/135GM11

700 Olabarrieta M, Geyer WR, Coco G, Friedrichs CT, Cao Z (2018) Effects of density-
701 driven flows on the long-term morphodynamic evolution of funnelshaped estuar-
702 ies. Journal of Geophysical Research: Earth Surface 123(11):2901–2924, DOI:
703 10.1029/2017JF004527

704 Partheniades E (1965) Erosion and deposition of cohesive soils. Journal of the Hy-
705 draulics Division, ASCE 91(1):105–139

706 Ralston DK (2005) Stratification and turbulence in subtidal channels through intertidal
707 mudflats. Journal of Geophysical Research 110(C8), DOI: 10.1029/2004JC002650

708 Ralston DK, Geyer WR, Traykovski PA, Nidzieko NJ (2013) Effects of estuarine and
709 fluvial processes on sediment transport over deltaic tidal flats. Continental Shelf Re-
710 search 60:S40–S57, DOI: 10.1016/j.csr.2012.02.004

711 Richardson LF (1920) The supply of energy from and to atmospheric eddies. Proceed-
712 ings of the Royal Society of London 97(686):354–373

713 Roelvink JA (2006) Coastal morphodynamic evolution techniques. Coastal Engineering
714 53(2-3):277–287, DOI: 10.1016/j.coastaleng.2005.10.015

715 Savenije H (2012) Salinity and Tides in Alluvial Estuaries, 2nd edn. Elsevier, New York

716 Scully ME, Friedrichs CT (2007) Sediment pumping by tidal asymmetry in a
717 partially mixed estuary. Journal of Geophysical Research 112(C7), DOI:
718 10.1029/2006JC003784

719 Shi JZ (2010) Tidal resuspension and transport processes of fine sedi-
720 ment within the river plume in the partially-mixed changjiang river estu-
721 ary, china: A personal perspective. Geomorphology 121(3):133–151, URL
722 http://www.sciencedirect.com/science/article/pii/S0169555X10002126

723 Shi JZ, Lu LF (2011) A short note on the dispersion, mixing, stratifica-
724 tion and circulation within the plume of the partially-mixed changjiang river
725 estuary, china. Journal of Hydro-environment Research 5(2):111–126, URL
726 http://www.sciencedirect.com/science/article/pii/S1570644310000675

727 Stelling GS, Van Kester JATM (1994) On the approximation of horizontal gradients in
728 sigma co-ordinates for bathymetry with steep bottom slopes. International Journal
729 for Numerical Methods in Fluids 18(10):915–935

730 Taylor GI (1931) Effect of variation in density on the stability of superposed
731 streams of fluid. Proceedings of the Royal Society of London Series A, Contain-

732 ing Papers of a Mathematical and Physical Character 132(820):499–523, DOI:
733 10.1098/rspa.1931.0115, URL https://doi.org/10.1098/rspa.1931.0115

734 Townend I (2012) The estimation of estuary dimensions using a simplified form model
735 and the exogenous controls. Earth Surf Processes Landf 37(15):1573–1583, DOI:
736 10.1002/esp.3256

737 Uncles RJ, Stephens JA (1996) Salt intrusion in the tweed estuary. Estuarine Coastal
738 & Shelf Science 43(3):271–293

739 Wang ZB, Louters T, Vriend HJD (1995) Morphodynamic modelling for a tidal in-
740 let in the Wadden Sea. Marine Geology 126(126):289–300, DOI: 10.1016/0025-
741 3227(95)00083-B

742 van der Wegen M, Jaffe B (2014) Processes governing decadal-scale depositional nar-
743 rowing of the major tidal channel in San Pablo Bay, California, USA. Journal of Geo-
744 physical Research: Earth Surface 119(5):1136–1154, DOI: 10.1002/2013JF002824

745 van der Wegen M, Roelvink J (2012) Reproduction of estuarine bathymetry by means
746 of a process-based model: Western Scheldt case study, the Netherlands. Geomor-
747 phology 179:152–167, DOI: 10.1016/j.geomorph.2012.08.007

748 van der Wegen M, Roelvink JA (2008) Long-term morphodynamic evolution of a
749 tidal embayment using a two-dimensional, process-based model. J Geophys Res
750 113(C3):C03,016, DOI: 10.1029/2006JC003983

751 van der Wegen M, Wang ZB, Savenije HHG, Roelvink JA (2008) Long-term morphody-
752 namic evolution and energy dissipation in a coastal plain, tidal embayment. J Geo-
753 phys Res 113(C3):F03,001, DOI: 10.1029/2007JF000898

754 van der Wegen M, Jaffe BE, Roelvink JA (2011) Process-based, morphodynamic hind-
755 cast of decadal deposition patterns in San Pablo Bay, California, 1856-1887. J Geo-
756 phys Res 116:F02,008–F02,008, DOI: 10.1029/2009JF001614

Winterwerp JC (2007) On the sedimentation rate of cohesive sediment. vol 8, Elsevier, pp 209–226

Zhang W, Cao Y, Zhu Y, Zheng J, Ji X, Xu Y, Wu Y, Hoitink AJF (2018) Unravelling the causes of tidal asymmetry in deltas. Journal of Hydrology 564:588–604, DOI: 10.1016/j.jhydrol.2018.07.023

Zhou Z, Coco G, Jiménez M, Olabarrieta M, van der Wegen M, Townend I (2014a) Morphodynamics of river-influenced back-barrier tidal basins: The role of landscape and hydrodynamic settings. Water Resources Research 50(12):9514–9535, DOI: 10.1002/2014WR015891

Zhou Z, Olabarrieta M, Stefanon L, D'Alpaos A, Carniello L, Coco G (2014b) A comparative study of physical and numerical modeling of tidal network ontogeny. Journal of Geophysical Research: Earth Surface 119(4):892–912, DOI: 10.1002/2014JF003092

Zhou Z, Stefanon L, Olabarrieta M, D'Alpaos A, Carniello L, Coco G (2014c) Analysis of the drainage density of experimental and modelled tidal networks. Earth Surface Dynamics 2(1):105–116, DOI: 10.5194/esurf-2-105-2014

Zhou Z, Coco G, van der Wegen M, Gong Z, Zhang C, Townend I (2015) Modeling sorting dynamics of cohesive and non-cohesive sediments on intertidal flats under the effect of tides and wind waves. Continental Shelf Research 104:76–91, DOI: 10.1016/j.csr.2015.05.010

Zhou Z, van der Wegen M, Jagers B, Coco G (2016) Modelling the role of self-weight consolidation on the morphodynamics of accretional mudflats. Environmental Modelling & Software 76:167–181, DOI: 10.1016/j.envsoft.2015.11.002

Zhou Z, Coco G, Townend I, Olabarrieta M, van der Wegen M, Gong Z, D'Alpaos A, Gao S, Jaffe B, Gelfenbaum G, He Q, Wang Y, Lanzoni S, Wang Z, Winterwerp H,

782 Zhang C (2017) Is “morphodynamic equilibrium” an oxymoron. Earth-Science Re-
783 views 165:257–267, DOI: 10.1016/j.earscirev.2016.12.002

784